ACS OMEGA

Open Access

http://pubs.acs.org/journal/acsodf

Article

Preparation and Evaluation of Aminomalononitrile-Coated Ca−Sr Metal−Organic Frameworks as Drug Delivery Carriers for Antibacterial Applications

Adhisankar Vadivelmurugan, Ramalingam Sharmila, Whei-Lin Pan, and Shiao-Wen Tsai*

Cite This: *ACS Omega* 2023, 8, 41909−41917

Read Online

ACCESS | Metrics & More | Article Recommendations

ABSTRACT: After orthopedic surgery, antibiotics are usually employed to reduce the risk of infection. If it is possible to enhance antimicrobial functionality and incorporate antimicrobial agents into the bone-filling matrix, not only it can promote bone tissue regeneration, but it can also enable localized administration of medication to elevate antibacterial efficacy. Meanwhile, previous studies have shown that calcium and strontium can support the growth of osteoblastic cells and diminish bone resorption or deterioration. In the past few years, metal−organic frameworks (MOFs) have been widely used as drug carriers owing to their characteristic advantages. In this study, a MOF was prepared in an aqueous solution by a simple coprecipitation method with the organic ligand 1,3,5-tricarboxylic benzene (H_3BTC) as a linker to form Ca−Sr−MOF. Furthermore, the Ca−Sr−MOF was coated with aminomalononitrile (AMN), which adhered through the electrostatic interactions between H_3BTC and AMN. With this MOF (Ca−Sr−AMN−MOF), AMN polymerization reactions can occur in aqueous environments, and a polymer layer was observed on the MOF surface with moderate hydrophilicity. The prepared Ca−Sr−MOF and Ca−Sr−AMN−MOF were characterized by Fourier transform infrared spectroscopy, powder X-ray diffraction, scanning electron microscopy, high-resolution transmission electron microscopy, and UV−visible spectroscopy. Finally, tetracycline (TC) was selected as the model drug to measure the drug loading efficiency, release profile, and antibiotic activity. The percent cumulative drug release of TC from Ca−Sr−MOF and Ca−Sr−AMN−MOF was 55.15 and 9.1%, respectively. The antibacterial effectiveness of TC-loaded MOF against Gram-negative *Escherichia coli* bacteria was evaluated, revealing the remarkable antimicrobial performance of these substances.

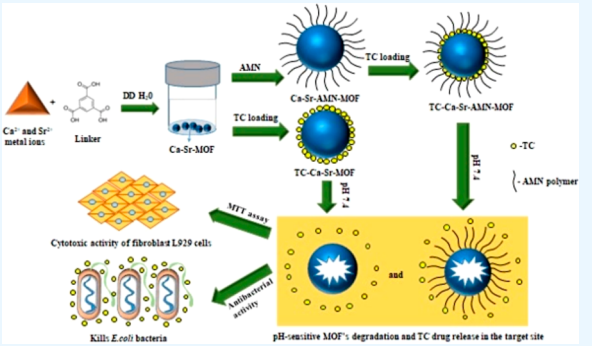

INTRODUCTION

With the development of antibacterial materials, nano- and microcarriers with great potential as therapeutics and drug delivery agents have been produced to enhance antibiotic efficacy and control bacterial resistance in specific cases.[1] Nanomaterial-based antibiotic drug delivery systems have numerous advantages over the administration of free antibiotics, including controlled and sustained drug release kinetics, ease of surface modification for bacterial targeting, infected site targeting, excellent localized bioactivity, reduced systemic side effects, ability to deliver multiple antibiotics, and heightened drug solubility and stability.[2]

Metal−organic frameworks (MOFs) are a type of organic−inorganic hybrid compound with one-, two-, or three-dimensional structural topologies containing inorganic metal ion clusters along with organic ligands.[3,4] Because of their tunable pore size, pore volume, high surface area, micro mesoporosity,[5] potential further chemical functionalization, simple surface modification, structural connectivity among their absorbed guest fragments, host structure, and excellent design ability,[6,7] MOFs have attracted attention and been widely used in the biomedical field, especially as drug carriers in drug delivery with antibacterial activities in recent years, due to their excellent drug loading capacity (LC) and drug release efficacy.[5,8,9] In the past few years, MOF-based nanomaterials have been increasingly used in antibacterial applications. Compared with conventional antibacterial agents, they have a few specific benefits: (1) bactericidal metal ions (e.g., Ag^+, Ca^{2+}, Sr^{2+}, Zn^{2+}, Co^{2+}, and Cu^{2+}), along with certain organic antimicrobials/natural bioantimicrobials (e.g., porphyrins and imidazoles) are suitable for fabricating MOFs, and these components can be viably released as required by modifying their water/acid/base stability under precise stimuli (e.g.,

Received: September 13, 2023
Revised: October 9, 2023
Accepted: October 12, 2023
Published: October 26, 2023

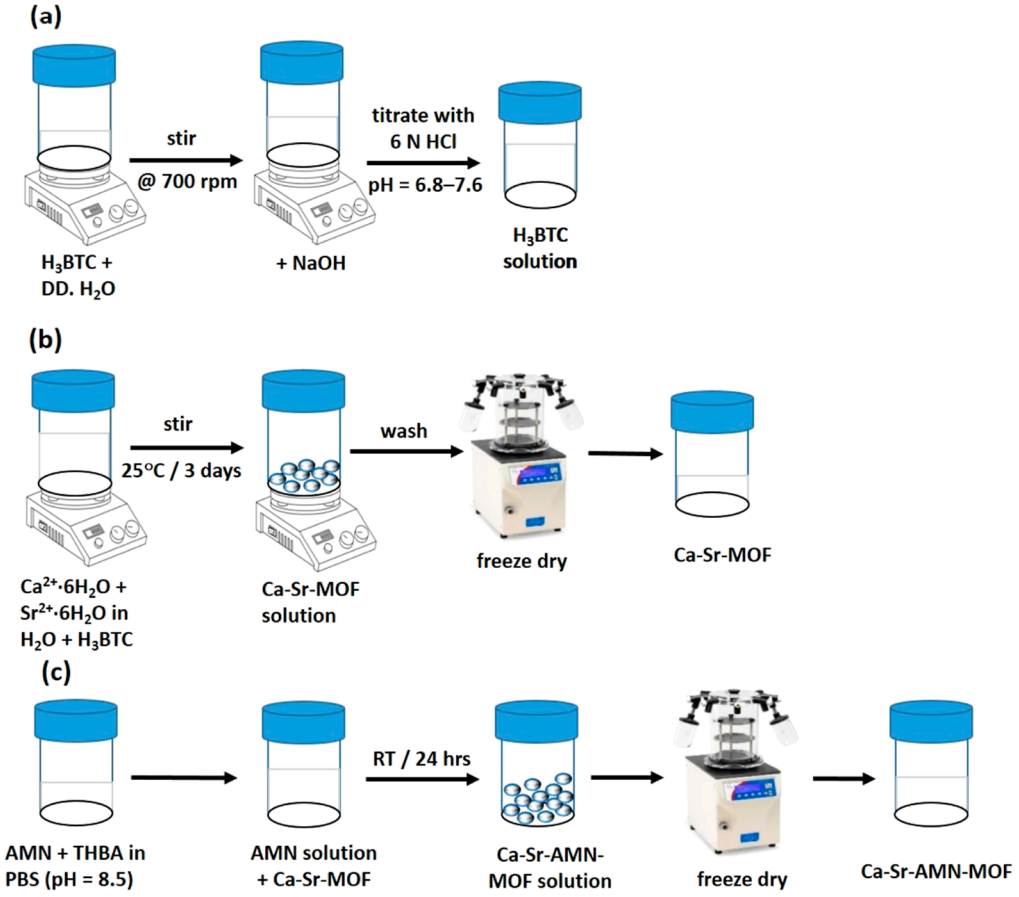

Figure 1. (a) Preparation of the H_3BTC solution. (b) Preparation of Ca−Sr−MOF. (c) Preparation of the AMN solution and Ca−Sr−AMN−MOF.

lowering pH and laser radiation).[10,11] (2) The chelation effect of MOFs reduces the polarity of their metal ions and therefore increases their lipophilicity, which allows MOFs to penetrate bacterial cell membranes and kill bacteria.[12]

Calcium and strontium can enhance osteoblastic cell development and reduce bone resorption or disintegration.[13] Furthermore, aminomalononitrile (AMN) coatings are a simple and versatile platform for biomolecule immobilization.[14] The exceptionally nitrogenous nature of AMN coatings allows them to act as an appropriate substrate for enhancing cell attachment, along with promoting metal ion immobilization, in applications varying from distinction to antimicrobial surface coatings.[15] In this study, a Ca−Sr−MOF was prepared in an aqueous solution via a simple precipitation method. To moderate the hydrophilicity, the Ca−Sr−MOF surface was coated with an AMN polymer. Thereafter, both the Ca−Sr−MOF and Ca−Sr−AMN−MOF were completely characterized by Fourier transform infrared (FTIR) spectroscopy, powder X-ray diffraction (PXRD), scanning electron microscopy (SEM), transmission electron microscopy (TEM), and UV−visible spectroscopy.

Antibacterial activity refers to any activity that kills bacteria or inhibits their growth or ability to replicate.[16] Tetracycline (TC) is a broad-spectrum antibiotic that demonstrates antibiotic activity against infections caused by both Gram-positive and Gram-negative microorganisms along with several kinds of bacteria.[17] To further evaluate the properties of Ca−Sr−MOF and Ca−Sr−AMN−MOF as drug carriers, the antibiotic drug TC was incorporated, and the drug release of TC in a pH 7.4 environment was evaluated. Furthermore, the successful loading of the antibiotic TC onto Ca−Sr−MOF and Ca−Sr−AMN−MOF was confirmed by FTIR and UV−visible spectroscopy. Finally, the antibiotic activity of TC loaded onto Ca−Sr−MOF and Ca−Sr−AMN−MOF against Gram-negative *Escherichia coli* bacteria was evaluated by the agar-well disc diffusion method.

MATERIALS AND METHODS

Materials. Calcium chloride hexahydrate ($Ca^{2+}·6H_2O$), strontium chloride hexahydrate ($Sr^{2+}·6H_2O$), trimeric acid, tetracycline hydrochloride, aminomalononitrile *p*-toluene sulfonate (98%), and 2,4,5-trihydroxy benzaldehyde (THBA, 99%) were purchased from Sigma-Aldrich. Dulbecco's modified Eagle's medium (DMEM), penicillin, sodium pyruvate, trypsin, and fetal bovine serum (FBS) were purchased from Gibco (Carlsbad, CA). L929 fibroblast cells and *E. coli* bacteria (BCRC 11634) were purchased from the BioSource collection and research center (BCRC, Taiwan). A 2000 Da dialysis membrane bag was purchased from Fischer Scientific. Luria−Bertani (LB) broth (LB medium), LB agar, and hydrochloric acid (37%) were purchased from Sigma-Aldrich. Unless otherwise noted, all other reagents and solvents were purchased from Sigma-Aldrich Chemical Co. (St. Louis, MO, USA). Other reagents and buffer solution components were of analytical grade. Double-distilled and deionized water (DD H_2O) was used in all experiments. All solutions and reagents were used without further purification. Figure 1 depicts a schematic illustration of the fabrication procedure.

https://doi.org/10.1021/acsomega.3c06991
ACS Omega 2023, 8, 41909−41917

Characterization of MOF Materials. *UV−Visible Spectroscopy.* The prepared Ca−Sr−MOF and Ca−Sr−AMN−MOF were resuspended in DD water with the 60 μg mL^{-1} concentration. UV−visible spectroscopy was employed to assess the MOF's maximum absorbance within the wavelength range of 200−900 nm (JASCO V-730, Japan). All of the measurements are repeated three times on each sample.

High-resolution Transmission Electron Microscopy. The prepared Ca−Sr−MOF and Ca−Sr−AMN−MOF were resuspended in DD water with the 60 μg mL^{-1} concentration. Samples were coated on a copper grid and subsequently subjected to drying. The morphological characteristics of the MOFs were captured by using high-resolution transmission electron microscopy (HR-TEM, JEM-2100, Japan).

Scanning Electron Microscopy. The prepared Ca−Sr−MOF and Ca−Sr−AMN−MOF were deposited on the aluminum specimen mounts, and ions were sputtered prior to the measurement. After ion sputtering, the images of the MOFs were acquired by using SEM (HITACHI, S-3000 N, Japan).

Fourier Transform Infrared Spectroscopy. The synthesized Ca−Sr−MOF and Ca−Sr−AMN−MOF were subjected to analysis using the attenuated total reflection method (ATR), which enables the direct measurement of small quantities of powder samples. The ATR method entails compressing the sample against a high-refractive-index prism and recording the infrared spectrum using infrared light that undergoes total internal reflection within the prism. The characteristics of the MOFs were assessed by using FTIR spectroscopy (Thermo Scientific TS5).

Powder X-ray Diffraction. The phase compositions of prepared Ca−Sr−MOF and Ca−Sr−AMN−MOF were characterized by a high-sensitivity modular X-ray diffractometer (Bruker AXS D2 Phaser, Germany) using Cu Kα radiation (λ = 0.154 Å, 40 kV, and 30 mA). The scanning region of the diffraction angle (2θ) was from 10 to 70°. All the measurements are repeated three times on each sample.

Preparation of Ca−Sr−MOF and Ca−Sr−AMN−MOF. Stock solutions of 100 mg/mL 1,3,5-tricarboxylic benzene (H_3BTC) were prepared by weighing 20 g of H_3BTC and adding it to a closed glass stock bottle. Then, 60 mL of DD H_2O was added to the bottle. The solution was placed on a stirring plate and stirred at 700 rpm. Sodium hydroxide (10 M) was continuously added to the solution, and H_3BTC was dissolved well. Finally, the solution was titrated with 6 N HCl until within a pH range of 6.8−7.6. DD H_2O was then added until the appropriate concentration was attained. One gram of $Ca^{2+}{\cdot}6H_2O$ and 1 g of $Sr^{2+}{\cdot}6H_2O$ were dissolved in 20 mL of DD H_2O and shaken well until completely dissolved. Then, 5 mL of a H_3BTC solution was added to the salt solution and gently stirred. This solution was maintained at 25 °C for up to 3 days for Ca−Sr−MOF crystallization, and the sample was washed with deionized water and then freeze-dried. The AMN solution was prepared by dissolving AMN and THBA at final concentrations of 2.76 and 11.8 mM in phosphate buffer solution (PBS, pH 8.5), respectively. Next, 8 mL of Ca−Sr−MOF aqueous solution (25 mg/mL) was added to 5 mL of AMN solution. This solution was then allowed to sit at room temperature for 24 h to form AMN-coated Ca−Sr−MOF crystals. The sample was washed with deionized water and then freeze-dried.

Determination of Drug Loading Capacity. TC was selected as the model drug to measure the drug loading efficiency and release profile. In brief, Ca−Sr−MOF (20 mg) and Ca−Sr−AMN−MOF (20 mg) were added to 2 mL of TC aqueous solution (10 mg/mL) and stirred for 24 h. The TC-loaded Ca−Sr−MOF and Ca−Sr−AMN−MOF were then collected by centrifugation, washed with deionized water, and freeze-dried. The concentration of TC was analyzed by UV−visible spectroscopy at a wavelength of 288 nm. The drug LC was calculated according to the following formula.

$$\text{Loading capacity (\%)} = \frac{\text{drug weight in carrier}}{\text{weight of carrier}} \times 100$$

Determination of Drug Release. TC-loaded Ca−Sr−MOF and Ca−Sr−AMN−MOF (20 mg) were lyophilized for drug release studies, placed into PBS solution at pH 7.4 (15 mL), and then agitated at 180 rpm with a paddle in a horizontal shaking bath at 37 °C. Then, 3 mL aliquots were taken manually from the buffer solution at predetermined time intervals for 24 h for measurement. The solution volume was replaced with fresh PBS at pH 7.4. The amount of drug present in the aliquots was measured by UV−visible spectroscopy. The cumulative TC release was calculated using the calibration curve of TC in PBS at 7.4 p H. Each experiment was performed in triplicate, and the average values and standard deviations were reported. The TC release profile was calculated with a determined TC standard calibration curve at 288 nm.

Determination of Cytotoxicity. Sample extracts were prepared according to the International Organization for Standardization 10993-5-2009. First, the extract solution was prepared at a concentration of 0.1 g 1 mL^{-1} in sterilized DMEM. Then, for the 3-(4,5-dimethylthiazol-2-yl)-2,5-diphenyltetrazolium bromide (MTT) assay, the L929 fibroblast cell line was cultured at a density of 1×10^4 cells/well in a 96-well plate and maintained in DMEM (Wisent Inc., USA) supplemented with 10% FBS (Wisent Inc.) and 1% sodium pyruvate (Wisent Inc.) at 37 °C in a humidified atmosphere with 5% CO_2. After a 24 h incubation, the cells were treated with test extracts, such as Ca−Sr−MOF, Ca−Sr−AMN−MOF, TC−Ca−Sr−MOF, TC−Ca−Sr−AMN−MOF, and free TC, and then incubated again at 37 °C in a humidified atmosphere with 5% CO_2. After a 24 h incubation, the cell viability was assayed using MTT. The optical density was measured at a wavelength of 570 nm. The percent cell viability was calculated using the following equation.

$$\text{Cell viability (\%)} = \frac{\text{OD570}_e}{\text{OD570}_b} \times 100$$

where $OD570_e$ is the mean value of the measured optical density of the sample extract and $OD570_b$ is the mean value of the measured optical density of the blanks.

Determination of Antimicrobial Activity. The antimicrobial activity of free TC, Ca−Sr−MOF, TC−Ca−Sr−MOF, Ca−Sr−AMN−MOF, and TC−Ca−Sr−AMN−MOF was measured via the agar-well diffusion technique, where fresh cultures of *E. coli* bacteria were used. Initially, 25 mL of Møller agar was incubated on sterilized Petri plates with the analogous strains of bacteria. The plates were left to solidify at room temperature for 2 days. To evaluate the antimicrobial activity, the materials were each prepared at a concentration of 10 mg mL^{-1} in a 0.1 M mL^{-1} HCl solution. Then, prepared 6 mm filter paper discs with 50 μL of free TC, Ca−Sr−MOF, TC−Ca−Sr−MOF, Ca−Sr−AMN−MOF, and TC−Ca−Sr−

https://doi.org/10.1021/acsomega.3c06991
ACS Omega 2023, 8, 41909−41917

AMN−MOF were administered onto the inoculated Mueller−Hinton agar surfaces. Then, the plates were incubated at 37 °C for 24 h, and the zones of inhibition were measured.

Statistical Analysis. The experiments were conducted in triplicate, and three parallel measurements for each sample were performed. The results were expressed as the means plus or minus the standard deviations. The statistical analysis to compare any significant difference between the groups was conducted with a *t*-test. $p < 0.05$ was considered statistically significant.

RESULTS AND DISCUSSION

Strontium-containing hydroxyapatite (SrHAP) has been demonstrated to not only improve the low degradation rate of HAP but also promote the osteogenic differentiation of mesenchymal stem cells. Since calcium and strontium are important elements of synthetic HAP as scaffolds for bone regeneration, if antibacterial drug-containing particles can be incorporated into Ca/Sr-HAP, the potential for infection will be reduced. Therefore, in the present study, we aimed to synthesize Ca−Sr−MOFs for use in drug delivery systems and *E. coli* antibacterial applications. Ca−Sr−MOF was first prepared by a coprecipitation method, followed by the introduction of ligand H_3BTC as a linker. Then, the MOF surface was modified with the AMN polymer to prepare Ca−Sr−AMN−MOF. Subsequently, the prepared drug carriers Ca−Sr−MOF and Ca−Sr−AMN−MOF were examined using a variety of techniques, such as FTIR, XRD, TEM, SEM, and UV−visible spectroscopy, and their drug release was evaluated by UV−visible spectroscopy. FTIR spectroscopic studies were performed in the wave range of 550−4000 cm^{-1}, as shown in Figure 2. In the FTIR spectrum of Ca−Sr−MOF, the peaks at

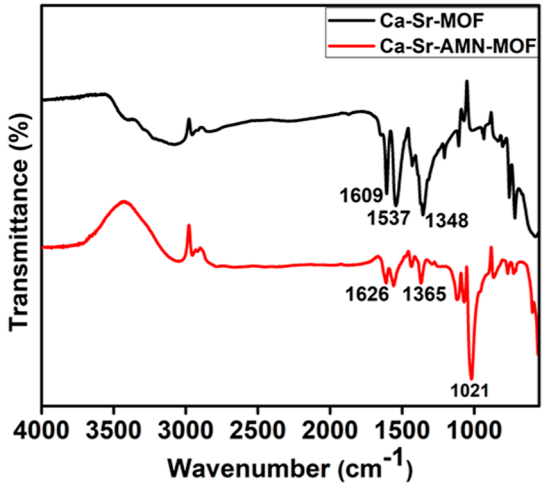

Figure 2. FTIR spectra of Ca−Sr−MOF and Ca−Sr−AMN−MOF.

strong vibrational bands at approximately 1609, 1537, and 1348 cm^{-1}, which are assigned to C═O, C−O and C−H vibrations, confirm the presence of the bridge coordination mode of Ca and Sr metal carboxylates in the Ca−Sr−MOF structures.[18,19] In the FTIR spectrum of Ca−Sr−AMN−MOF, the strong peaks at approximately 1626 and 1365 cm^{-1} are attributed to C═O and C−H vibrations, and a new peak at approximately 1021 cm^{-1} is attributed to the weak aliphatic amine (C−N) bond of AMN.[20] Moreover, the FTIR spectrum results indicate the successful preparation of Ca−Sr−MOF and Ca−Sr−AMN−MOF.

The PXRD technique was used to verify the structure of the prepared microparticles. The PXRD patterns of Ca−Sr−MOF and Ca−Sr−AMN−MOF are shown in Figure 3. In the PXRD

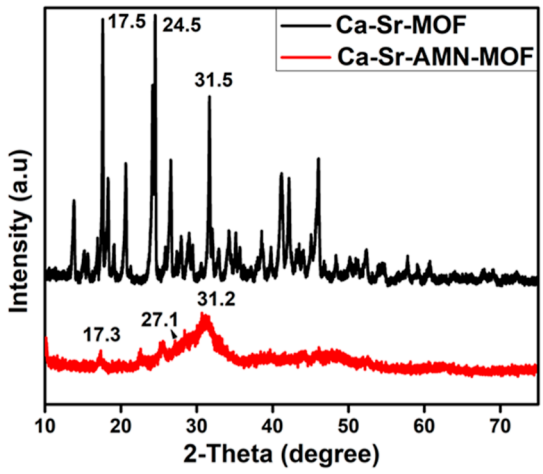

Figure 3. PXRD patterns of the synthesized Ca−Sr−MOF and Ca−Sr−AMN−MOF.

pattern of Ca−Sr−MOF, the sharp peaks of the crystal pattern indicate a crystalline phase. Furthermore, the sharp peaks of the crystal pattern that appear at 2θ = 17.50, 24.50, and 31.50, which are attributed to Ca and Sr ions, are a strong indication of the successful formation of Ca−Sr−MOF according to previous reports.[21] The PXRD pattern of Ca−Sr−AMN−MOF shows a large, broad peak in the crystal pattern, indicating an amorphous phase. Furthermore, the peaks at 2θ = 17.30 and 27.10 are attributed to the NH_4−CN group of the AMN polymer, which indicates an orderly pore structure, as confirmed by previous reports.[22,23] These PXRD results confirm the successful preparation of Ca−Sr−MOF and Ca−Sr−AMN−MOF.

The morphologies of the synthesized Ca−Sr−MOF and Ca−Sr−AMN−MOF were observed by SEM and HR-TEM. The image of Ca−Sr−MOF shown in Figure 4a shows a rod-like porous structure.[24] Moreover, after coating AMN onto the Ca−Sr−MOF, the morphology was altered, and a small threadlike structure appeared, as shown in Figure 4b.

The optical properties of the synthesized Ca−Sr−MOF and Ca−Sr−AMN−MOF were analyzed by UV−visible spectroscopy, as shown in Figure 5. The prepared materials exhibit UV−visible absorption spectra in the range of 250−500 nm. The difference in the maximum absorbances of Ca−Sr−MOF and Ca−Sr−AMN−MOF is due to their characteristic electronic configurations. In the UV−visible spectra of Ca−Sr−MOF, the maximum absorbance appears at 290 nm, which corresponds to the $\pi-\pi^*$ absorption of the MOF, as per previous reports.[25,26] Moreover, in the UV−visible spectrum of Ca−Sr−AMN−MOF, the maximum absorbance appears at approximately 290 and 363 nm. This redshift may occur because the Ca^{2+} and Sr^{2+} metal ions of the MOF form complex with the amine groups of AMN, resulting in metal−amine complexes. These results are in good agreement with those of previous reports.[27]

Before the drug release experiment, the drug LC of TC in TC−Ca−Sr−MOF and TC−Ca−Sr−AMN−MOF was calcu-

https://doi.org/10.1021/acsomega.3c06991
ACS Omega 2023, 8, 41909−41917

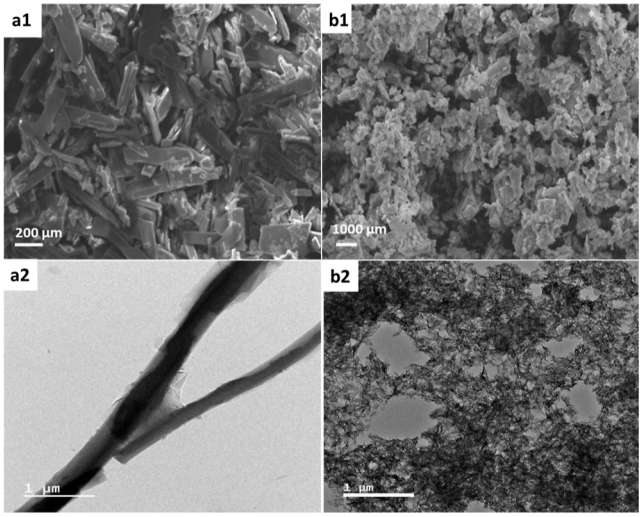

Figure 4. (a1) SEM image of Ca−Sr−MOF, (a2) HR-TEM image of Ca−Sr−MOF, (b1) SEM image of Ca−Sr−AMN−MOF, and (b2) HR-TEM image of Ca−Sr−AMN−MOF.

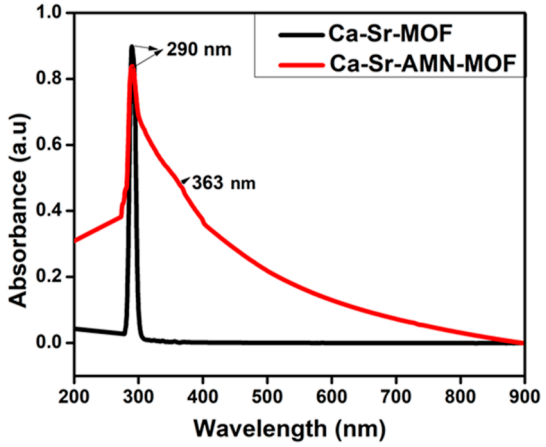

Figure 5. UV−visible spectra of Ca−Sr−MOF and Ca−Sr−AMN−MOF.

lated, and the results were 63 and 57%, respectively. Successful TC loading onto the Ca−Sr−MOF and Ca−Sr−AMN−MOF was confirmed by characterization with FTIR and UV−visible spectroscopy. First, FTIR spectroscopic studies were performed for all the materials in the wave range of 550−4000 cm^{-1}. The FTIR spectrum of pure TC is shown in Figure 6a, and the corresponding peaks due to the presence of OH and NH_2 groups are observed at 3353 cm^{-1}. In addition, the peak at 3041 cm^{-1} is attributed to the C−H stretching vibrations of aromatic rings, the peaks from 1572 to 1620 cm^{-1} are attributed to C═C stretching, the peak at 1214 cm^{-1} is attributed to C−N stretching, the peak at 1630 cm^{-1} is attributed to C═O stretching, and the peaks from 1037 to 1113 cm^{-1} are attributed to C−O stretching.[28,29] In addition, in the FTIR spectrum of TC−Ca−Sr−MOF, the peaks with strong vibrational bands at approximately 1601, 1510, and 1396 cm^{-1}, which are attributed to C═O, C−O, and C−H vibrations, confirm the presence of the bridge coordination mode of Ca and Sr metal carboxylates in the MOF structures. The absorption band at 3308 cm^{-1} is attributed to the NH_2 moiety of TC, indicating the successful loading of TC onto the Ca−Sr−MOF structure.[30,31] Moreover, in the FTIR spectrum of TC−Ca−Sr−AMN−MOF, absorption bands are noted at approximately 1598 and 1451 cm^{-1}, which are attributed to C═O and C−H vibrations, and an absorption band is noted at approximately 1024 cm^{-1}, which is attributed to the weak aliphatic amine bond (C−N) of AMN.[20] The absorption band at 3345 cm^{-1} is attributed to the NH_2 moiety of TC, indicating the successful loading of TC onto the Ca−Sr−AMN−MOF structure.[30−32] Moreover, the FTIR spectrum results confirm the successful loading of TC onto Ca−Sr−MOF and Ca−Sr−AMN−MOF. As shown in Figure 6b, the characteristic maximum absorbances of TC are 297 and 363 nm, which are values similar to those in previous reports.[30,33] Moreover, the TC peaks of TC−Ca−Sr−MOF and TC−Ca−Sr−AMN−MOF are 295 and 357 and 294 and 357 nm, respectively, which are blue-shifted from the native TC peaks of 297 and 363 nm. This blueshift may be a consequence of TC having a high possibility of forming chelation complexes with Ca^{2+} and Sr^{2+} metal ions, which are present in TC−Ca−Sr−MOF and TC−Ca−Sr−AMN−MOF. The NH_2 group of TC forms a coordination complex with these divalent cations.[34,35]

Ca−Sr−MOF and Ca−Sr−AMN−MOF were then used as drug carriers, and TC was selected as a model drug for evaluating the drug release of these MOFs. The solution was removed from the drug release setup, and UV was measured at

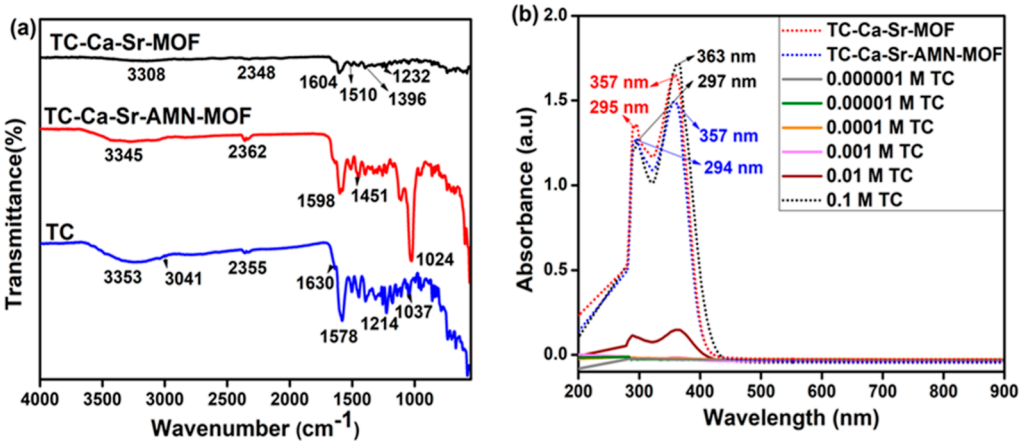

Figure 6. (a) FTIR spectra of pure TC, TC−Ca−Sr−MOF, and TC−Ca−Sr−AMN−MOF, (b) UV−visible spectra of the different molar concentrations of TC, TC−TC−Ca−Sr−MOF, and TC−Ca−Sr−AMN−MOF used to construct the calibration curve.

https://doi.org/10.1021/acsomega.3c06991
ACS Omega 2023, 8, 41909−41917

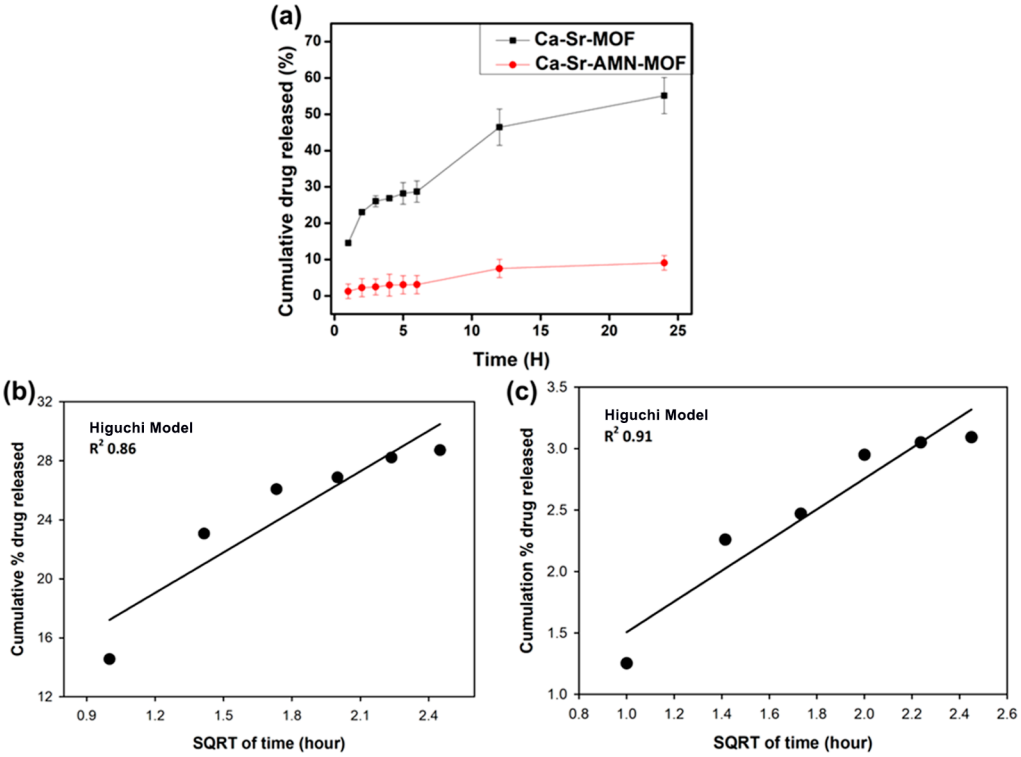

Figure 7. (a) Cumulative drug release (%) of TC from TC−Ca−Sr−MOF and TC−Ca−Sr−AMN−MOF at 37 °C in pH 7.4 PBS. (b,c) Curves of TC−Ca−Sr−MOF and TC−Ca−Sr−AMN−MOF fitted with the equation of the Higuchi model, respectively. Data are represented as the means ± SDs, n = 3.

predetermined intervals for 24 h. The TC release from TC−Ca−Sr−MOF and TC−Ca−Sr−AMN−MOF increases steadily over time for the following reasons: (1) the coordination between the divalent metal ions and ligand is destroyed under physiological pH due to the design of the MOFs.[10,36] (2) There is a possibility of breaking the complexation between divalent metal ions (Ca^{2+}, Sr^{2+}) of MOFs with the $-NH_2$ group of TC under neutral pH.[37] These factors finally lead to the destruction of the MOF structure, resulting in a faster and more significant release of TC from TC−Ca−Sr−MOF and TC−Ca−Sr−AMN−MOF. Moreover, the percent cumulative drug release of TC from TC−Ca−Sr−MOF is higher than that from TC−Ca−Sr−AMN−MOF, as shown in Figure 7a. The percent cumulative drug release of TC from TC−Ca−Sr−MOF and TC−Ca−Sr−AMN−MOF is 55.15 and 9.1%, respectively. In addition, the Higuchi model was used to analyze the release profile at an early stage because our system condition was fit to the Higuchi model requirements, such as negligible edge effects, initial concentration higher than drug solubility, dosage form larger than drug molecule, and perfect sink condition. As shown in Figure 7, the R squared (coefficient of determination) values were 0.86 and 0.91 for TC−Ca−Sr−MOF and TC−Ca−Sr−AMN−MOF, respectively. Other released models were used to fit the released data, but all R squared values were lower than those of the Higuchi model.

The cytotoxicity of prepared materials used for biomedical applications is the most critical factor that can reduce their adverse side effects. The effect of the prepared MOFs without TC was evaluated in vitro to ensure that the MOFs did not have an independent toxicity effect. Hence, the cytotoxicity of the synthesized drug carriers Ca−Sr−MOF and Ca−Sr−AMN−MOF was assessed by an MTT assay. In this part, the relative cell viability was more than 80% for Ca−Sr−MOF and Ca−Sr−AMN−MOF, as shown in Figure 8a, which indicated

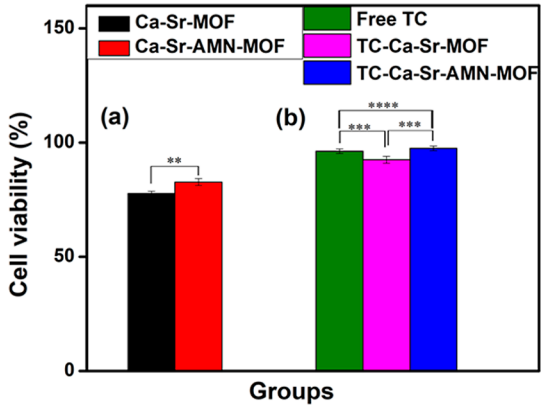

Figure 8. (a) MTT assay for Ca−Sr−MOF and Ca−Sr−AMN−MOF and (b) MTT assay for free TC, TC−Ca−Sr−MOF, and TC−Ca−Sr−AMN−MOF. The data are represented as the mean ± standard deviation (n = 3). For all charts, ****: $p < 0.0001$; ***: $p < 0.001$; **: $p < 0.01$; *: $p < 0.05$ according to the t-test.

that neither Ca−Sr−MOF nor Ca−Sr−AMN−MOF exhibited any toxicity toward L929 fibroblast cells.[38] Moreover, the effects of free TC, TC−Ca−Sr−MOF, and TC−Ca−Sr−AMN−MOF on the proliferation of L929 fibroblast cells were evaluated by the MTT assay, the results of which are shown in Figure 8b. No reduced cell viability was observed following incubation with each prepared material. These MTT results demonstrate the biocompatibility of free TC, TC−Ca−Sr−

https://doi.org/10.1021/acsomega.3c06991
ACS Omega 2023, 8, 41909−41917

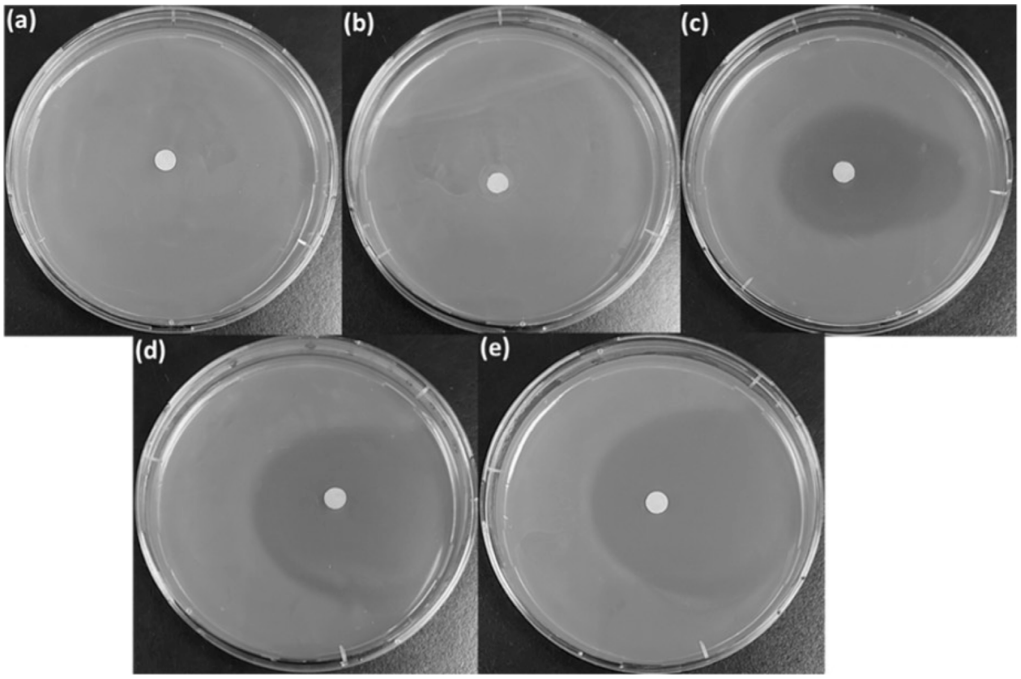

Figure 9. Zones of inhibition of *E. coli* plates containing discs of (a,b) Ca−Sr−MOF and Ca−Sr−AMN−MOF and (c,e) pure TC, TC−Ca−Sr−MOF, and TC−Ca−Sr−AMN−MOF.

MOF, and TC−Ca−Sr−AMN−MOF, which show no toxicity toward L929 fibroblast cells.[32,39]

The antimicrobial activities of free TC, Ca−Sr−MOF, TC−Ca−Sr−MOF, Ca−Sr−AMN−MOF, and TC−Ca−Sr−AMN−MOF were determined with a standard *E. coli* strain. In this experiment, the diameter of the zone of inhibition was assessed after incubation to determine the antimicrobial activity. As shown in Figure 9, the radii of the zones of inhibition of TC−Ca−Sr−MOF, TC−Ca−Sr−AMN−MOF, and pure TC against *E. coli* bacteria were 40.5 ± 0.5, 44.5 ± 0.5, and 30.3 ± 0.2 mm, respectively. No obvious inhibition zone was observed for Ca−Sr−MOF and Ca−Sr−AMN−MOF. The antibacterial mechanism is associated with the gradual disintegration of the MOF structure and release of metal ions, organic ligands, and drugs (TC), resulting in damage to membranes and fragmentation of DNA, causing cell wall damage and death.[10,40] Here, the AMN coating and the antibiotic-loaded MOF synergistically exert antibacterial activity, leading to a larger inhibition zone of TC−Ca−Sr−AMN−MOF.[41] These results reveal that the use of Ca−Sr−MOF and Ca−Sr−AMN−MOF as drug carriers can enhance the antibacterial activity of TC.

CONCLUSIONS

Bacterial infections have consistently remained a frequent issue after clinical surgeries. Consequently, recent research has been a growing focus on developing antimicrobial surfaces for implants, aiming to not only minimize infections but also promote cellular adhesion and proliferation. In addition, localized sustained drug delivery systems can decrease the required medication dosage while amplifying antibacterial effects. Moreover, despite the strong biocompatibility, bioactivity, and osteoconductivity of synthetic hydroxyapatite, the incorporation of strontium enhances degradability compared with the traditional hydroxyapatite form, thereby promoting osteogenesis. In this study, we successfully fabricated Ca−Sr−MOF and Ca−Sr−AMN−MOF materials and incorporated TC into MOFs for drug delivery and *E. coli* antibacterial applications. The cumulative drug release of TC from TC−Ca−Sr−MOF and TC−Ca−Sr−AMN−MOF was 55.15 and 9.1%, respectively, after 24 h. Meanwhile, the Higuchi model can be used to explain the release profile at the early stage. In addition, by performing an MTT assay, both the MOF and TC-loaded MOF have no significant cytotoxicity. Finally, the antibiotic activity order is TC−Ca−Sr−AMN−MOF > TC−Ca−Sr−MOF > TC, which indicates that the antibiotic activity can be enhanced by MOF structure effects and complex compositions. Together, these results show that Ca−Sr−MOF and Ca−Sr−AMN−MOF prepared in the study have potential for biomedical applications, particularly surface modification for bone implants.

AUTHOR INFORMATION

Corresponding Author

Shiao-Wen Tsai − *Department of Biomedical Engineering, Chang Gung University, Taoyuan 33302, Taiwan; Department of Periodontics, Chang Gung Memorial Hospital, Taipei 10507, Taiwan;* orcid.org/0000-0002-6225-6613; Email: swtsai@mail.cgu.edu.tw

Authors

Adhisankar Vadivelmurugan − *Department of Biomedical Engineering, Chang Gung University, Taoyuan 33302, Taiwan*

Ramalingam Sharmila − *Department of Biomedical Engineering and Environmental Sciences, National Tsing Hua University, Hsinchu 300044, Taiwan*

Whei-Lin Pan − *Department of Periodontics, Chang Gung Memorial Hospital, Taipei 10507, Taiwan*

Complete contact information is available at: https://pubs.acs.org/10.1021/acsomega.3c06991

https://doi.org/10.1021/acsomega.3c06991
ACS Omega 2023, 8, 41909−41917

Funding

The present research was supported by Chang Gung Memorial Hospital, grant number CMRPD2K0152, and Chang Gung University, grant number BMRP633.

Notes

The authors declare no competing financial interest.

■ ACKNOWLEDGMENTS

The authors thank the Microscopy Center at Chang Gung University for technical assistance.

■ REFERENCES

(1) Makabenta, J. M. V.; Nabawy, A.; Li, C. H.; Schmidt-Malan, S.; Patel, R. M.; Rotello, V. Nanomaterial-based therapeutics for antibiotic-resistant bacterial infections. *Nat. Rev. Microbiol.* **2021**, *19*, 23−36.

(2) Osman, N.; Devnarain, N. A.; Omolo, C.; Fasiku, V.; Jaglal, Y.; Govender, T. Surface modification of nano-drug delivery systems for enhancing antibiotic delivery and activity. *Wiley Interdiscip. Rev.: Nanomed. Nanobiotechnol.* **2022**, *14*, 1758.

(3) Serre, C.; Millange, F.; Surble, S.; Ferey, G. A route to the synthesis of trivalent transition-metal porous carboxylates with trimeric secondary building units. *Angew. Chem., Int. Ed.* **2004**, *43*, 6285−6289.

(4) Liu, R.; Yu, T.; Shi, Z.; Wang, Z. The preparation of metal–organic frameworks and their biomedical application. *Int. J. Nanomed.* **2016**, *11*, 1187−1200.

(5) Horcajada, P.; Gref, R.; Baati, T.; Allan, P. K.; Maurin, G.; Couvreur, P.; Ferey, G.; Morris, R. E.; Serre, C. Metal-organic frameworks in biomedicine. *Chem. Rev.* **2012**, *112*, 1232−1268.

(6) Keskin, S.; Kizilel, S. Biomedical applications of metal organic frameworks. *Ind. Eng. Chem. Res.* **2011**, *50*, 1799−1812.

(7) Ma, Z.; Moulton, B. Recent advances of discrete coordination complexes and coordination polymers in drug delivery. *Coord. Chem. Rev.* **2011**, *255*, 1623−1641.

(8) He, S.; Wu, L.; Li, X.; Sun, H.; Xiong, T.; Liu, J.; Huang, C.; Xu, H.; Sun, H. W.; Chen, W.; Gref, R.; Zhang, J. Metal-organic frameworks for advanced drug delivery. *Acta Pharm. Sin. B* **2021**, *11*, 2362−2395.

(9) Cai, M.; Chen, G.; Qin, L.; Qu, C.; Dong, X.; Ni, J.; Yin, X. Metal Organic Frameworks as Drug Targeting Delivery Vehicles in the Treatment of Cancer. *Pharmaceutics* **2020**, *12*, 232.

(10) Nasrabadi, M.; Ghasemzadeh, M. A.; Zand Monfared, M. R.; Monfared, R. The Preparation and Characterization of UiO-66 Metal-Organic Frameworks for the Delivery of the Drug Ciprofloxacin and an Evaluation of Their Antibacterial Activities. *New J. Chem.* **2019**, *43*, 16033−16040.

(11) Zhang, Y.; Sun, P.; Zhang, L.; Wang, Z.; Wang, F.; Dong, K.; Liu, Z.; Ren, J.; Qu, X. Silver-Infused Porphyrinic Metal-Organic Framework: Surface-Adaptive, On-Demand Nanoplatform for Synergistic Bacteria Killing and Wound Disinfection. *Adv. Funct. Mater.* **2019**, *29*, 1808594.

(12) Tweedy, B. G. Plant Extracts with Metal Ions as Potential Antimicrobial Agents. *Phytopathology* **1964**, *55*, 910−918.

(13) Li, M.; He, P.; Wu, Y.; Zhang, Y.; Xia, H.; Zheng, Y.; Han, Y. Stimulatory effects of the degradation products from Mg-Ca-Sr alloy on the osteogenesis through regulating ERK signaling pathway. *Sci. Rep.* **2019**, *6*, 32323.

(14) Thissen, H.; Koegler, A.; Salwiczek, M.; Easton, C. D.; Qu, Y.; Lithgow, T.; Evans, R. A. Prebiotic-chemistry inspired polymer coatings for biomedical and material science applications. *NPG Asia Mater.* **2015**, *7*, 225.

(15) Ball, V.; Toh, R. J.; Voelcker, N. H.; Thissen, H.; Evans, R. A. Electrochemical deposition of aminomalonitrile based films. *Colloids Surf., A* **2018**, *552*, 124−129.

(16) Balasubramaniam, B.; Prateek; Ranjan, S.; Saraf, M.; Kar, P.; Singh, S. P.; Thakur, V. K.; Singh, A.; Gupta, R. K. Antibacterial and Antiviral Functional Materials. Chemistry and Biological Activity Toward Tackling COVID-19-like Pandemics. *ACS Pharmacol. Transl. Sci.* **2021**, *4*, 8−54.

(17) Daghrir, R.; Drogui, P. Tetracycline antibiotics in the environment: a review. *Environ. Chem. Lett.* **2013**, *11*, 209−227.

(18) Vu, T. A.; Le, G. H.; Dao, C. D.; Dang, L. Q.; Nguyen, K. T.; Nguyen, Q. K.; Dang, P. T.; Tran, H. T. K.; Duong, Q. T.; Nguyen, T. V.; Lee, G. D. Arsenic removal from aqueous solutions by adsorption using novel MIL-53(Fe) as a highly efficient adsorbent. *RSC Adv.* **2015**, *5*, 5261−5268.

(19) Panda, R.; Rahut, S.; Basu, J. K. Preparation of a Fe2O3/MIL-53(Fe) composite by partial thermal decomposition of MIL-53(Fe) nanorods and their photocatalytic activity. *RSC Adv.* **2016**, *6*, 80981−80985.

(20) Li, J.; Jiao, Y.; Feng, L.; Zhong, Y.; Zuo, G.; Xie, A.; Dong, W. Highly N, P-doped carbon dots: Rational design, photoluminescence and cellular imaging. *Microchim. Acta* **2017**, *184*, 2933−2940.

(21) Joseph, N.; Lawson, H. D.; Overholt, K. J.; Damodaran, K.; Gottardi, R.; Acharya, A. P.; Little, S. R.; Little, S. R. Synthesis and characterization of Ca Sr-Metal Organic Frameworks for biodegradable orthopedic applications. *Sci. Rep.* **2019**, *9*, 13024.

(22) Ruiz-Bermejo, M.; de la Fuente, J. L.; Carretero-Gonzalez, J.; Garcia-Fernandez, L.; Aguilar, M. R. A Comparative Study on HCN Polymers Synthesized by Polymerization of NH_4CN or Diaminomaleonitrile in Aqueous Media: New Perspectives for Prebiotic Chemistry and Materials Science. *Chem.—Eur. J.* **2019**, *25*, 11437−11455.

(23) Ruiz-Bermejo, M.; de la Fuente, J. L.; Pérez-Fernández, C.; Mateo-Martí, E. A Comprehensive Review of HCN-Derived Polymers. *Processes* **2021**, *9*, 597.

(24) Wu, Y.; Pang, H.; Yao, W.; Wang, X.; Yu, S.; Yu, Z.; Wang, X. Synthesis of rod-like metal-organic framework (MOF-5) nanomaterial for efficient removal of U(VI): batch experiments and spectroscopy study. *Sci. Bull.* **2018**, *63*, 831−839.

(25) Jin, Z.; Yang, H. Exploration of Zr-Metal-Organic Framework as Efficient Photocatalyst for Hydrogen Production. *Nanoscale Res. Lett.* **2017**, *12*, 539.

(26) Gao, Y.; Hilbers, M.; Zhang, H.; Tanase, S. Designed Synthesis of Multiluminescent Materials Using Lanthanide Metal-Organic Frameworks and Carbon Dots as Building-Blocks. *Eur. J. Inorg. Chem.* **2019**, *2019*, 3925−3932.

(27) Abinaya, M.; Muthuraj, V. Bi-functional catalytic performance of silver Manganite/polypyrrole nanocomposite for electrocatalytic sensing and photocatalytic degradation. *Colloids Surf., A* **2020**, *604*, 125321.

(28) Sanaei-Rad, S.; Ghasemzadeh, M. A.; Razavian, S. M. H. Synthesis of a novel ternary ZIF-8/GO/MgFe2O4 nanocomposite and its application in drug delivery. *Sci. Rep.* **2021**, *11*, 18734.

(29) Zhang, X.; Liu, L.; Huang, L.; Zhang, W.; Wang, R.; Yue, T.; Sun, J.; Li, G.; Wang, J. The highly efficient elimination of intracellular bacteria via a metal organic framework (MOF)-based three-in-one delivery system. *Nanoscale* **2019**, *11*, 9468−9477.

(30) Anbazhagan, S.; Thangavelu, K. P. Application of tetracycline hydrochloride loaded-fungal chitosan and Aloe vera extract based composite sponges for wound dressing. *J. Adv. Res.* **2018**, *14*, 63−71.

(31) Darvishi, S.; Javanbakht, S.; Heydari, A.; Kazeminava, F.; Gholizadeh, P.; Mahdipour, M.; Shaabani, A. Ultrasound-assisted synthesis of MIL-88(Fe) coordinated to carboxymethyl cellulose fibers: A safe carrier for highly sustained release of tetracycline. *Int. J. Biol. Macromol.* **2021**, *181*, 937−944.

(32) Niamlang, P.; Tongrain, T.; Ekabutr, P.; Chuysinuan, P.; Supaphol, P. Preparation, characterization and biocompatibility of poly (vinyl alcohol) films containing tetracycline hydrochloride-loaded quaternized chitosan nanoparticles. *J. Drug Delivery Sci. Technol.* **2017**, *38*, 36−44.

(33) Zhang, X.; Liu, L.; Huang, L.; Zhang, W.; Wang, R.; Yue, T.; Sun, J.; Li, G.; Wang, J. The highly efficient elimination of intracellular bacteria via a metal organic framework (MOF)-based three-in-one delivery system. *Nanoscale* **2019**, *11*, 9468−9477.

https://doi.org/10.1021/acsomega.3c06991
ACS Omega 2023, 8, 41909−41917

(34) Ghadim, E. E.; Manouchehri, F.; Soleimani, G.; Hosseini, H.; Kimiagar, S.; Nafisi, S. Adsorption Properties of Tetracycline onto Graphene Oxide: Equilibrium, Kinetic and Thermodynamic Studies. *PLoS One* **2013**, *8*, No. e79254.
(35) Jeon, M.; Rhee Paeng, I. Quantitative detection of tetracycline residues in honey by a simple sensitive immunoassay. *Anal. Chim. Acta* **2008**, *626*, 180−185.
(36) Guerra, W.; Silva-Caldeira, P. P.; Terenzi, H.; Pereira-Maia, E. C. Impact of metal coordination on the antibiotic and non-antibiotic activities of tetracycline-based drugs. *Coord. Chem. Rev.* **2016**, *327*−*328*, 188−199.
(37) Chahardahmasoumi, S.; Sarvi, M. N.; Jalali, S. A. H. Modified montmorillonite nanosheets as a nanocarrier with smart pH responsive control on the antimicrobial activity of tetracycline upon release. *Appl. Clay Sci.* **2019**, *178*, 105135.
(38) Tian, H.; Zhang, M.; Jin, G.; Jiang, Y.; Luan, Y. Cu-MOF chemodynamic nanoplatform via modulating glutathione and H2O2 in tumor microenvironment for amplified cancer therapy. *J. Colloid Interface Sci.* **2021**, *587*, 358−366.
(39) Marson Armando, R. A.; Abuçafy, M. P.; Graminha, A. E.; Silva, R. S. d.; Frem, R. C. G. Ru-90@bio-MOF-1: A ruthenium(II) metallodrug occluded in porous Zn-based MOF as a strategy to develop anticancer agents. *J. Solid State Chem.* **2021**, *297*, 122081.
(40) Wyszogrodzka, G.; Marszałek, B.; Gil, B.; Dorozynski, P. Metal-organic frameworks: mechanisms of antibacterial action and potential applications. *Drug Discovery Today* **2016**, *21*, 1009−1018.
(41) Liao, T.-Y.; Easton, C. D.; Thissen, H.; Tsai, W.-B. Aminomalononitrile-Assisted Multifunctional Antibacterial Coatings. *ACS Biomater. Sci. Eng.* **2020**, *6*, 3349−3360.

https://doi.org/10.1021/acsomega.3c06991
ACS Omega 2023, 8, 41909−41917